Nuclear Instruments and Methods in Physics Research A321 (1992) 275-283
North-Holland

NUCLEAR INSTRUMENTS & METHODS IN PHYSICS RESEARCH
Section A

Multidisk neutron velocity selectors

Boualem Hammouda

Reactor Radiation Division, Materials Science and Engineering Laboratory, National Institute of Standards and Technology, Gaithersburg, MD 20899, USA

Received 28 February 1992 and in revised form 15 April 1992

Helical multidisk velocity selectors used for neutron scattering applications have been analyzed and tested experimentally. Design and performance considerations are discussed along with simple explanation of the basic concept. A simple progression is used for the inter-disk spacing in the "Rosta" design. Ray tracing computer investigations are presented in order to assess the "coverage" (how many absorbing layers are stacked along the path of "wrong" wavelength neutrons) and the relative number of neutrons absorbed in each disk (and therefore the relative amount of gamma radiation emitted from each disk). We discuss whether a multidisk velocity selector can be operated in the "reverse" configuration (i.e. the selector is turned by 180° around a vertical axis with the rotor spun in the reverse direction). Experimental tests and calibration of a multidisk selector are reported together with evidence that a multidisk selector can be operated in the "reverse" configuration.

1. Introduction

Monochromation is essential for non time-of-flight neutron scattering, and can be achieved by using either Bragg diffraction from crystals or using velocity selectors [1–3]. Until a few years ago, velocity selectors used a drum-based concept, whereby neutrons are allowed to travel through a helical slot; only those neutrons of the "right" speed are transmitted, the others (referred to as having the "wrong" wavelength) being absorbed because their speeds are either too slow or too fast. Multidisk velocity selectors (fig. 1) based on the "Rosta" design have become commercially available [4–7]. The main advantage is that they are lighter than their drum-based counterparts and are therefore easier and safer to drive to higher speeds to achieve better wavelength resolution and shorter wavelengths. In this paper, we review the concept and analyze their performance.

Some of the velocity selectors that have been manufactured [8] (Transelektro, Hungary) have their motor on the neutron entrance side (disks are closer on that side), while others have been built with the motor on the opposite side. For shielding and minimization of the neutron guide cut considerations, the second motor configuration seems more favorable. The question whether a multidisk velocity selector can be operated in the "reverse" configuration (i.e. the selector is turned around but the same helicity is kept) has been raised recently at the National Institute of Standards and Technology Cold Neutron Research Facility (NIST-CNRF) prompted by the acquisition of three non-identical selectors. The "reverse" configuration is achieved in practice by turning the selector by 180° about a vertical axis (so that neutrons enter through the opposite window) and the rotor is spun in the reverse direction by switching the current supplying wires of the driving motor. The first two NIST-CNRF selectors have their motors on the neutron entrance side (where disks are closely spaced), while the third has its motor on the other side. We wish to use the three selectors interchangeably, but prefer to avoid the required engineering to reverse and rebalance the rotor of the third selector. We have undertaken the task of understanding whether a multidisk selector can be operated in the "reverse" configuration before we were able to perform experimental tests. Design considerations, as well as performance assessment, are discussed. A ray tracing computer method has been used to analyze a specific selector (Rosta design [4–7]) and answer relevant questions. Moreover, recently, experimental tests

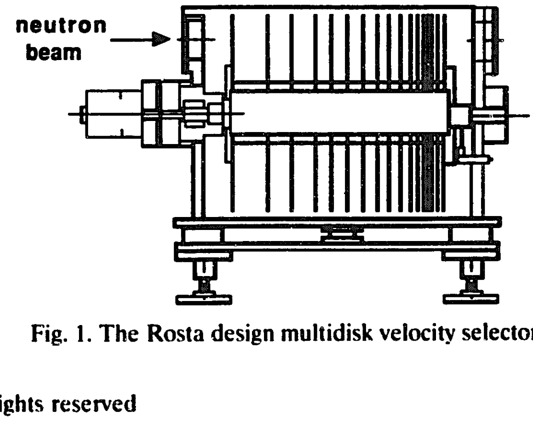

Fig. 1. The Rosta design multidisk velocity selector.

have been performed on a multidisk selector at NIST-CNRF and are reported here.

2. Wavelength, wavelength spread and transmission

Consider a perfectly collimated neutron beam parallel to the axis of a multidisk velocity selector that has n disks. The selector has a number of windows on each disk, with absorbing material between the windows. The angular width of the windows (at their mid height) is 2β, while the absorber (gadolinium oxide paint) width between two windows is 2δ. The selector rotates at a frequency ω (which is varied to change the wavelength): it has a length L (distance between the first and last disks), a helix pitch angle α and a radius R (to the middle of the windows). The wavelength of the transmitted neutrons λ is obtained by setting the time that it takes for the neutrons to travel the length L equal to the time that it takes for the selector to rotate by an angle α. This gives

$$\lambda = \alpha h / L m \omega,$$

where h and m are Planck's constant and the neutron mass. In more practical units, this formula reads:

$$\lambda[\text{Å}] = 6.59 \times 10^5 \alpha[\text{deg}]/[L[\text{mm}]\omega[\text{rpm}]].$$

We define two properties of the selector. The transmission T is proportional to the uncovered beam area on the disks:

$$T = 2\beta/(2\beta + 2\delta).$$

The wavelength resolution $\Delta\lambda/\lambda$ (defined here as the base of a triangular distribution) is proportional to the window width 2β and inversely proportional to the pitch angle α:

$$\Delta\lambda/\lambda = 2\beta/\alpha.$$

Note that this relative spread is independent of wavelength, so that the incoming λ^{-5} Maxwellian flux distribution tail from neutron moderators gives rise to a λ^{-4} dependence in the current density distribution after traversing the selector.

In order to improve the wavelength resolution, one can either make 2β smaller or α larger. The first possibility is limited by the mechanical integrity of the disks because 2δ must also be made small proportionately for constant transmission. The second alternative (increase of the pitch angle) results in an increase in the selected wavelength; so that a higher rotation speed is required to obtain the same wavelength. This puts higher constraints on the driving motor and increases the possibility of damage of the selector bearings. A third alternative is to increase the length L of the selector proportionately to the increase of the pitch angle, thereby leaving the wavelength range unshifted.

In order to vary the wavelength spread, the selector axis is tilted horizontally by an angle ν relative to the beam axis. The consequence is a modification of the pitch angle to give an effective value:

$$\alpha_{\text{eff}} = \alpha + \nu L/R.$$

Tilting of the selector not only modifies the wavelength spread but also changes the mean wavelength. Moreover, the effect of coarse neutron collimation is to increase α_{eff}, so that an average over the angular distribution of the incoming neutron beam is required.

3. Distribution of the disks along the neutron path

The transmission of neutrons with spurious wavelength is avoided by a judicious choice of the distribution of the disks along the selector axis. In order to close all possible pathways for these parasitic wavelengths, it is useful to consider the neutron moving frame and define a relative "wavelength" variable (fig. 2):

$$X = (\alpha/L) - (\omega\lambda m/h),$$

which represents an angle (in the vertical plane of the disks) per unit length (along the selector rotation axis) for a specified wavelength λ. The value $X = 0$ defines the "right" (transmitted) wavelength represented by an "open" channel in the moving frame of the neutron in which the disks appear as stationary. All other values

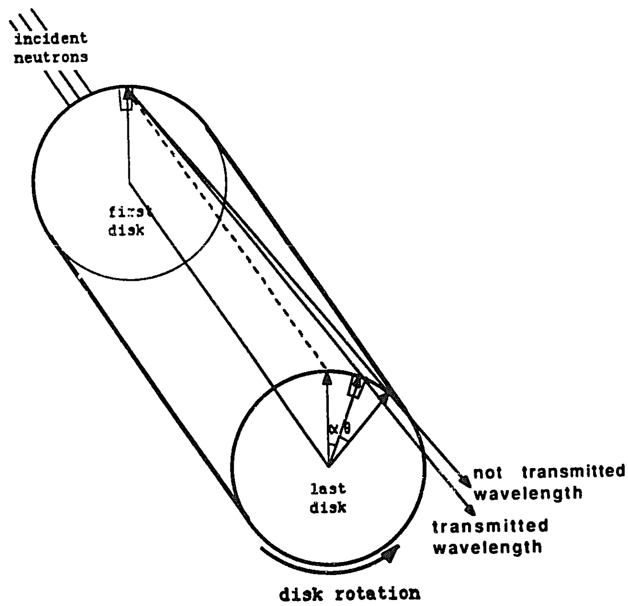

Fig. 2. Some neutron trajectories and angle definitions. α is the helix pith angle for the selector and θ is the angle of rotation of the last disk during the time it takes for a neutron to transverse the selector (i.e. to travel from the first disk to the last one).

of X define "wrong" wavelengths that are blocked by the insertion of additional disks between the first and last ones. Figs. 2 and 3 represent schematically the open channel ($X = 0$) (also called transmitting channel), together with other closed ones that are represented by lines such as OL, OM, ON, etc, in fig. 3 and that correspond to "wrong" wavelength neutrons. Note that ray OM, for example, has an angle $\theta_i = l_i X$ associated with it in the disk plane (θ is defined in fig. 2). This angle θ_i is the angle of rotation of disk i during the time that the considered neutron travels the distance from the first disk to disk i. θ_i varies linearly with the distance from the first disk (this distance is denoted by l_i at the position of disk i) and with the wavelength λ (through X). Here the disk index i is allowed to vary from $i = 1$ for the first disk to $i = n$ for the last one. One would like to ensure that neutrons of the "wrong" wavelength never reach the last disk.

One possible scheme for constructing a distribution of disk spacings (the Rosta design [4–6]) considers only one absorbing/transmitting pair of (adjacent) channels (see fig. 3). Consider a "wrong" wavelength λ characterized by an angle θ_i. If the angle θ_i is set equal to $2\beta + \delta$, neutrons of wavelength λ end up in the middle of an absorbing region in disk i (for example, point M is at the middle of segment HS in fig. 3). Actually, this scheme can be implemented starting from the last disk and working backward. As shown in fig. 3, drawing a line OL to the last disk ($i = n$) yields the point H (intersection of OL and QG) which is the location of disk $n - 1$, the intersection of OM with QG yields point K which is the location of disk $n - 2$, and so on, down to the second disk ($i = 2$). The location of disks i and $i - 1$ (distances l_i's are measured with respect to the first disk at the neutron entrance side) are therefore related by:

$$l_{i-1}/l_i = 2\beta/(2\beta + \delta),\ i = 3, \ldots, n,$$

starting with $l_n = L$ and proceeding backward. This progression reduces the disk spacing at the neutron entrance side and is truncated by having n disks.

This scheme of distributing the disks along the axis is not unique. It has been referred to as a "double coverage" approach [4–6], meaning that each "wrong" wavelength neutron must cross at least two absorbing layers (except for the first and the last disks which have double the neutron absorbing thickness). As can be seen in fig. 3, this is not the case and a few single

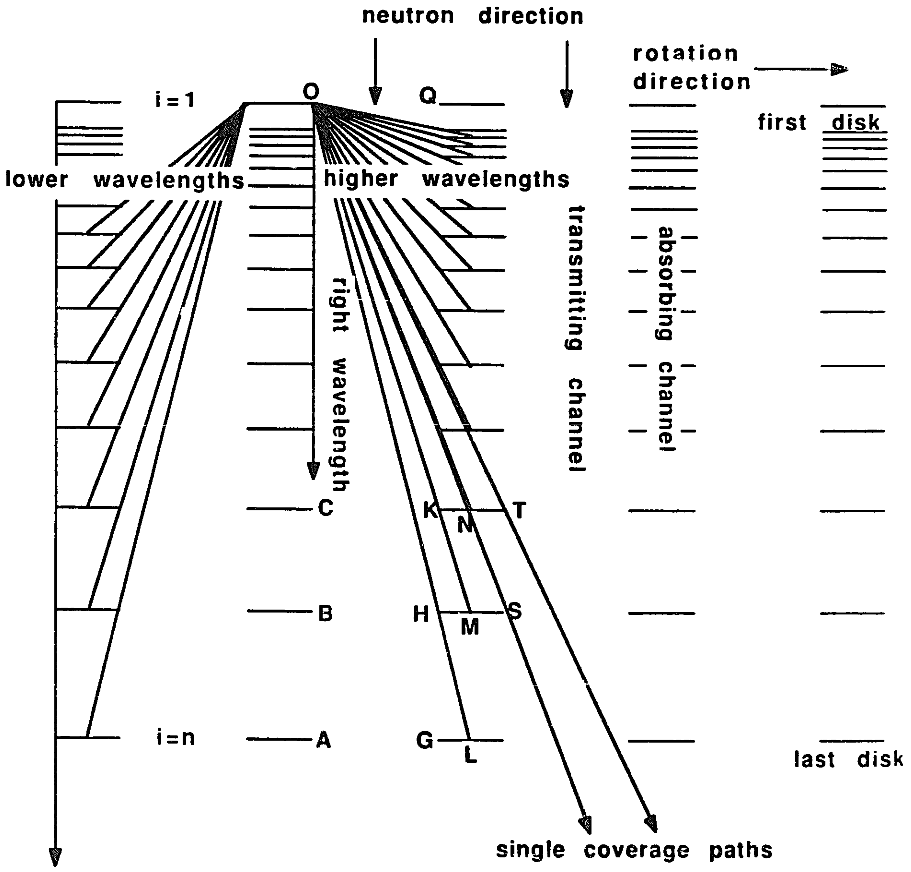

Fig. 3. Distribution of the disks along the velocity selector symmetry axis in the relative frame of the neutron. Wrong wavelength neutrons are shown incident with nonzero relative angles. Two single coverage paths are shown with arrows.

coverage paths can be found geometrically. Moreover, one can show that, given two neighboring disks i and $i-1$ (located, say, at B and C in fig. 3), the difference in angles (BOS)-(BON) in the plane of fig. 3 is always negative:

$$\begin{aligned}(\mathrm{BOS})-(\mathrm{BON}) &= R(2\beta+2\delta)/l_i - R(2\beta+\delta)/l_{i-1} \\ &= (R/l_i)\left[(2\beta+2\delta)-(2\beta+\delta)^2/2\beta\right] \\ &= -R\delta^2/2\beta l_i < 0.\end{aligned}$$

This means that such single coverage channels are systematic. Note that the plane of fig. 3 corresponds to a cylindrical surface around the outer edges of the disks. Single coverage paths can occur for wavelengths λ:

$$\lambda/\lambda_0 = 1 \pm [(2\beta+2\delta)/\alpha](2\beta+\delta)^{n-i}/(2\beta)^{n-i}.$$

where λ_0 is the "right" wavelength. This criterion has been verified graphically (fig. 3) for disks not far from the neutron exit side. Four single coverage path "islands" occur between the first and second transmitting/absorbing channels (two of them are shown in fig. 3). It seems that these four are the only single coverage regions because the coverage becomes necessarily higher than one when trajectories have wide angles in the plane of fig. 3.

A ray tracing computer program has been written to follow the trajectory of neutrons and record the number of disks "crossed" in order to reach the last disk. This is done by stepping over a range in θ angles and checking whether and how many absorbing regions fall on the trajectory. The "coverage" for each wrong wavelength path is obtained. Figs. 4a, 4b and 4c show the coverage when neutrons are incident on the "forward" side (where disk spacing is tight) and when the selector is used in the "reverse" configuration. These figures have been plotted using the following velocity selector parameters corresponding to the NIST third selector: $L = 420$ mm, $n = 22$, $\beta = 0.9375°$, $\delta = 0.3125°$, and with 1000 neutrons crossing the selector. Note that in the moving frame of the neutron (plane of fig. 3), the value of the pitch angle α is not required in order to estimate the coverage. Fig. 4b, for example, shows the four single coverage regions. The variation of the coverage is seen to vary steeply from step to step; this is due to the fact that all considered neutrons originate from the outer edge of the window (as shown in fig. 3). If we consider a uniform illumination whereby the initial position of the neutron is averaged over the window width, we find smoother variations of the coverage. The main trends of this variation are, however, expected to remain unchanged. At large values of θ, the coverage number approaches a finite value which is proportional to the total number of disks n and to the probability of hitting an absorbing region on each disk

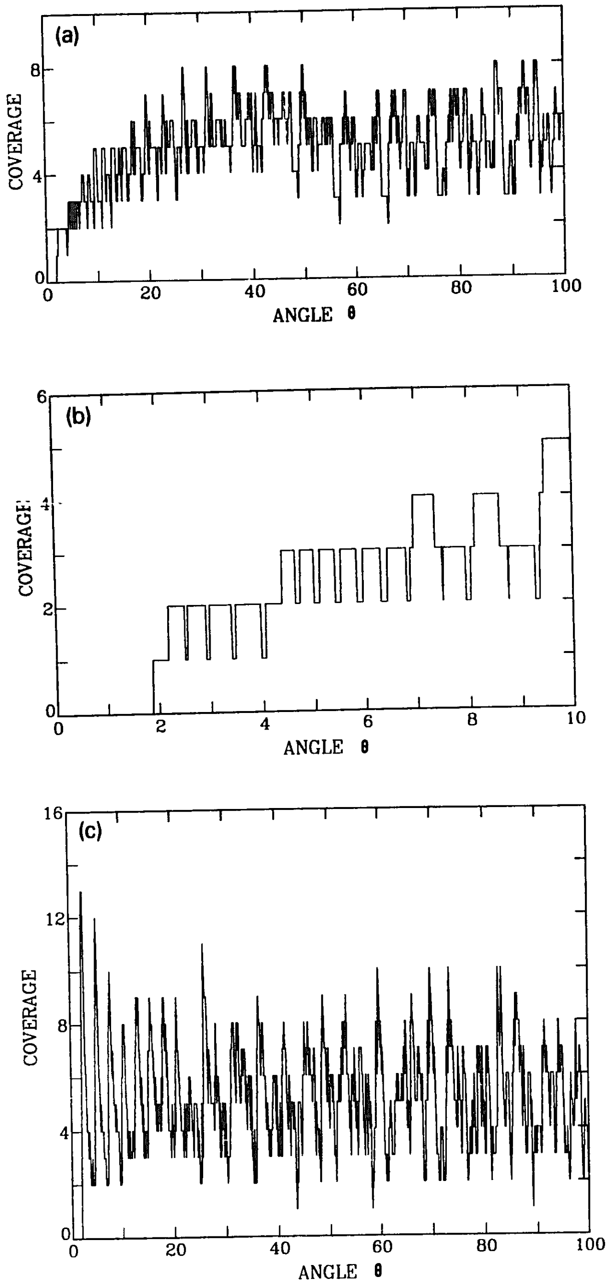

Fig. 4. (a) Variation of the coverage (i.e. number of disks "crossed") with angle θ (that represents neutron wavelength) in the "forward" configuration (i.e. disks are closely spaced on the neutron entrance side). (b) Expansion of a part of (a) with higher resolution (smaller θ step size). The four single-coverage islands (coverage = 1) appear clearly. (c) Variation of the coverage (i.e., number of disks "crossed") with angle θ (representing the neutron wavelength) in the "reverse" configuration (i.e. when the selector is turned 180° about a vertical axis and its rotor spun in the reverse direction). No zero coverage path is observed.

$(\delta/(\delta+\beta))$. In our numerical application, this limit is 5.5. Fig. 4c shows that no zero coverage path exists when the selector is used in the "reverse" configuration.

4. Distribution of the stopped wavelengths

The goal of this section is to explain which disks stop which wavelengths and to the calculated wavelength spread of the transmitted neutrons. The angle θ_i, for a given neutron path, is defined as positive in a clockwise direction in the vertical plane of disk i (fig. 2). Neutrons of wavelengths shorter than the transmitted wavelength are characterized by positive θ_i's (represented on the left side of fig. 3) and have a low cutoff value corresponding to $\lambda = 0$, while longer wavelengths are characterized by negative θ_i's and are available for arbitrarily high λ's. For this reason, the first few disks (close to the neutron entrance side) stop long wavelength neutrons, intermediate disks stop short wavelengths while the last disks (where disk spacing is wider) stop neutrons of wavelengths close to the transmitted one.

Disk i stops on the average (based on the middle of the absorbing region 2δ) neutrons of wavelength:

$$\lambda = [(\alpha/L) \pm (2\beta + \delta)/l_i] h/m\omega$$
$$= \left[(\alpha/L) \pm (2\beta + \delta)^{n-i+1}/(2\beta)^{n-i}L)\right] h/m\omega,$$

where l_i has been replaced by:

$$l_i = L[2\beta/(2\beta + \delta)]^{n-i}.$$

For instance, the zero wavelength corresponds to disk i_0 where:

$$i_0 = n + \log[\alpha/2\beta]/\ln[(2\beta + \delta)/2\beta] \text{ (for } \lambda = 0).$$

This zero wavelength case corresponds to "photon propagation" and is therefore a selector at rest (zero rotation frequency) with absorption occurring at disk i_0 instead of $i = 1$. We assume that the rays originate at the edge of a window and require a distance corresponding to the first i_0 disks to meet the other edge of the same window (recall that we are assuming a perfectly collimated neutron beam parallel). Because of symmetry considerations the same disk i_0 also stops neutrons that have twice the transmitted wavelength.

The choice of a number of disks n (this includes the first one located at $l_1 = 0$) is equivalent to a truncation of the progression which therefore determines a relationship between the long wavelength cutoff λ_c and the transmitted wavelength λ_0:

$$\lambda_c/\lambda_0 = 1 + (2\beta + \delta)^n/(2\beta)^{n-1}\alpha.$$

This cutoff wavelength is usually sufficiently high that the neutron flux at that wavelength is negligible. This scheme of distributing the disks considers only two adjacent transmitting/absorbing channels, but of course the other (next nearest neighbor and higher) channels stop neutrons of wavelengths higher than the cutoff. Moreover, when the disks become very close to each other (at the neutron entrance side) their finite thickness starts blocking a non-negligible solid angle.

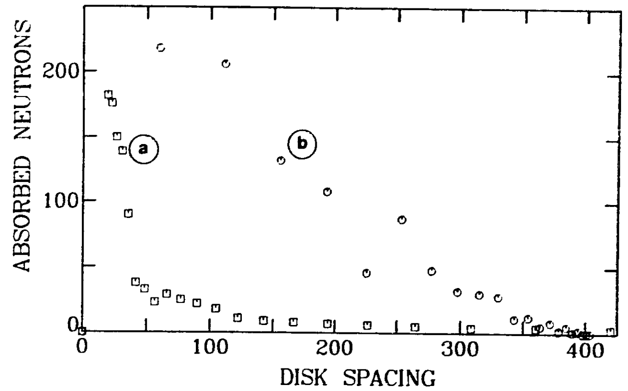

Fig. 5. Relative fractions of "wrong" wavelengths stopped by each disk. Curves a and b correspond to the "forward" and "reverse" configurations respectively.

The relative wavelength spread stopped by the full 2δ width of the absorbing region of disk i corresponds to:

$$\Delta\lambda_i/\lambda_i = 2\delta/(2\beta + \delta)$$

centered around λ_i. The ray tracing program has also been used to obtain the fraction of wavelengths stopped by each disk (assuming absorption at the first encounter with a disk). The incident wavelength distribution is assumed uniform and only wavelengths larger than the transmitted wavelength (λ_0) have been considered for simplicity. Wavelengths that are shorter than the transmitted wavelength give a distribution of absorbed neutrons that is identical to the portion λ_0 to $2\lambda_0$. Fig. 5 shows such distributions in the "forward" and "reverse" configurations. Such distributions when generalized to include a nonuniform Maxwellian neutron spectrum can be useful in the design of gamma shields around the selector. When operated in the "forward" configuration, the selector absorbs neutrons (therefore emitting gamma radiation) mainly at and around the first disk, while operation in the "reverse" configuration causes the neutron absorption to be more evenly distributed along the selector. It is noted that the sum of the ordinate values in fig. 5 for all disks is the same in the "forward" and "reverse" configurations and is equal to the total number of absorbed neutrons (proportional to $\delta/(\beta + \delta)$). Fig. 5 has been plotted using the velocity selector parameters mentioned in the previous section and given in section 5.

5. Numerical application

Consider the following selector parameters corresponding to the third NIST-CNRF velocity selector: $L = 420$ mm, $R = 176$ mm, $\alpha = 20°$, $2\beta = 1.875°$, $2\delta = 0.625°$ and $n = 22$. This gives a transmission of $T = 75\%$ and a wavelength spread of $\Delta\lambda/\lambda = 9.375\%$ for $\nu = 0$.

Single coverage paths are found to occur for $i = 20$ at $\lambda/\lambda_0 = 1 \pm 0.145$ (ray OS in fig. 3) and for $i = 19$ at $\lambda/\lambda_0 = 1 \pm 0.17$ (ray OT in fig. 3), for example. All four single coverage "islands" (fig. 4b) are close to the transmitted wavelength but outside of the instrument resolution width. Single coverage is, however, good enough that no spurious wavelengths are transmitted as will be discussed in the experimental section below. The choice of $n = 22$ yields a cutoff wavelength ratio $\lambda_c/\lambda_0 = 4.4$. Also, we calculate that $i_0 = 6$ which means that the zero wavelength case corresponds to the 6th disk which is located at $l_6 = 41$ mm from the neutron entrance side.

6. Discussion

We now discuss whether a multidisk selector can be operated in the "reverse" configuration. If we reverse both the velocity of the neutrons and the direction of rotation of the rotor, all of the above treatment holds exactly with the redefinition of the velocities $v' = -v$ and angles $\alpha' = -\alpha$. The diagrams given in fig. 3 remain the same. Neutrons do not care about the distribution of the disks inside the selector; if they have the "wrong" wavelength, they are absorbed whether they correspond to v and θ or to v' and θ'. Instead of being absorbed by the neighboring absorbing channel,

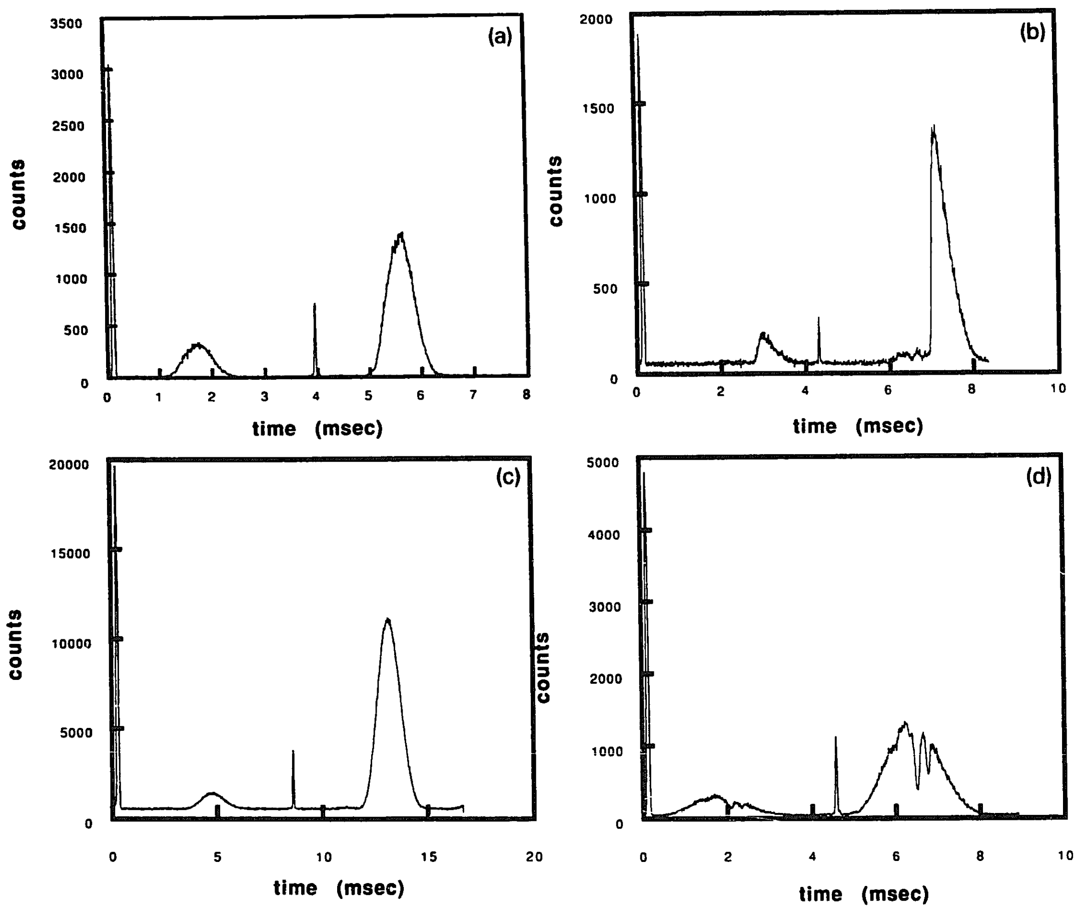

Fig. 6. (a) Time-of flight calibration curve (counts vs flight time) for a selector rotation speed of 5000 rpm, at zero tilt angle ($\nu = 0$) and for a Fermi chopper rotation frequency of 260 Hz. The two broad peaks are detected by two detectors and the two sharp ones are due to the "reverse" burst in the Fermi chopper. Intensities are on an arbitrary scale. (b) Time-of flight calibration curve (counts vs flight time) for a selector rotation speed of 5000 rpm, at zero tilt angle ($\nu = 0$) and for a Fermi chopper rotation frequency of 240 Hz. The sharp leading edge of a 5 cm thick polycrystalline graphite piece can be observed on both peaks. (c) Time-of flight calibration curve (counts vs flight time) for a selector rotation speed of 3000 rpm, at +3° tilt angle and for a Fermi chopper rotation frequency of 120 Hz. This corresponds to a wavelength above the Bragg cutoff for Bi. (d) Time-of flight calibration curve (counts vs flight time) for a selector rotation speed of 2500 rpm, at −3° tilt angle and for a Fermi chopper rotation frequency of 225 Hz. This corresponds to a wavelength below the Bragg cutoff for Bi so that diffraction dips can be observed.

they travel some distance before meeting an absorbing region, and the inherent design ensures that these meet such a region. Obviously, if the selector is rotated in the forward direction, it should not transmit neutrons at all. However, in this case, the cutoff wavelength is shifted. For example, for the set of selector parameters considered before, λ_c/λ_0 becomes equal to 2.4 (instead of the value 4.4), and some long wavelength neutrons can be observed (and have been observed at LLB-Saclay during a spurious test run [9]) because the flux at λ_c would be only $(2.5)^5 = 80$ times lower than at λ_0 (in the previous section, this number was $(4.4)^5 = 1649$).

7. Experimental tests and calibration

Experimental tests and calibration of the multidisk velocity selector whose design parameters are described in the numerical section have been performed at the NIST-CNRF. These measurements have been performed on the 30 m small angle neutron scattering (SANS) instrument which is located on guide NG7. This instrument uses cold neutrons that are filtered though 15 cm of Be. Also a 15 cm thick Bi crystal is used as a gamma filter. This crystal has a few large grains which can Bragg diffract neutrons below a cutoff wavelength of 7.9 Å.

7.1. Experimental arrangement and method used

A standard time-of-flight method is used to test and calibrate the multidisk velocity selector. This involves measuring the time taken for neutrons to travel a well defined distance. The experimental arrangement consists of the multidisk selector in its shield housing (steel enclosure filled with wax, borax and iron shot and lead bricks). The SANS instrument collimation consists of a 15 m long evacuated neutron flight path containing eight 1.5 m Ni coated guides that can be moved into the beam therefore shortening the source-to-sample distance. For the purpose of maximizing count rates most of our measurements have been performed with six guides in the beam, with a source-to-sample distance of 6.45 (0.275° beam divergence). A Fermi chopper was placed at the instrument sample position in order to start neutron bursts which are subsequently monitored by two detectors: one pencil detector with

Table 1
Results of the experimental tests and calibration of the third NIST-CNRF multidisk velocity selector. σ_t is the standard deviation of the flight time distribution

ω [rpm]	ν [deg]	$t_2 - t_1$ [μs]	λ_0 [Å]	σ_t [μs]	S_λ/λ [%]
2000	0	13,469	13.23	605	8.98
2500	0	10,830	10.63	488	9.02
3000	0	8,996	8.83	404	9.0
3500	0	7,783	7.64	351	9.02
4000	0	6,855	6.73	298	8.7
4500	0	6,024	5.91	263	8.74
5000	0	5,499	5.40	235	8.56
2500	+3	15,582	15.30	604	7.76
3000	+3	12,928	12.69	500	7.74
4000	+3	9,788	9.61	380	7.76
5000	+3	7,836	7.69	298	7.6
1800	−3	8,566	8.41	775	18.1
2000	−3	7,713	7.57	693	17.96
2500	−3	6,286	6.17	594	18.9
3000	−3	5,259	5.16	429	16.3
1800	−2	10,445	10.26	725	13.88
2100	−2	8,918	8.76	631	14.16
2500	−2	7,572	7.43	523	13.82
3000	−2	6,248	6.13	460	14.72
3500	−2	5,440	5.34	358	13.14
1800	−1	13,080	12.84	680	10.4
2100	−1	11,205	11.00	583	10.42
3500	−1	6,875	6.75	349	10.14
2500	+1	12,080	11.86	500	8.28
3500	+1	8,683	8.53	359	8.26
5000	+1	6,074	5.96	246	8.08

low efficiency immediately after the chopper ($d_1 = 82.6$ mm) and the main SANS instrument area detector located at $d_2 = 4112$ mm from the chopper. Counts from these two detectors (only total counts from the area detector were used) were fed into an electronics counting chain consisting of histogramming memories that can record sequentially (up to 1024) time slices (channels) of adjustable size. The recorded spectra (counts vs time) show the two main peaks (centered around t_1 and t_2) corresponding to the two detectors (see fig. 6a). The spectra also show two "reverse burst" peaks because the Fermi chopper with its broad slot width has a direct line of sight for neutrons transmitted in the middle of the rotation period. The neutron wavelength is obtained from the values of t_1 and t_2 using the relation:

$$\lambda = 3962(t_2 - t_1)/(d_2 - d_1),$$

where λ is in Å, t's are in μs and d's are in mm. Peak widths are also extracted using a weighted sum of the counts around the second detector peak.

7.2. Tests and calibration

Section 5 gives the parameters of the selector used for these tests in the "reverse" configuration. The first tests, therefore, consist of a series of runs with fixed selector rotation speed (5000 rpm) and variable Fermi chopper frequency in order to scan the wavelength range. The following observations are made: 1) no spurious peaks due to the transmission of wrong wavelengths are observed, and 2) no spurious peaks due to single coverage along the path of wrong wavelength neutrons are observed in the wings of the main peaks.

As an independent check of the method used to determine the wavelength, polycrystalline graphite (50 mm thick) with a sharp Bragg edge at 6.73 Å was placed after the selector. Using the Fermi chopper method, this edge was found to be located at 6.76 ± 0.02 Å (shown in fig. 6b) for a selector rotation speed of 4000 rpm.

Next, a series of runs were taken at various selector speeds (up to 5000 rpm), corresponding Fermi chopper frequencies and time channel widths and various selector tilt angles ranging from $-3°$ to $+3°$. The measurements are summarized in table 1 along with the corresponding wavelengths and relative wavelength spreads extracted. Note that the FWHM of the peak recorded by the second detector, S_λ, is related to the standard deviation σ_λ of the distribution (which is assumed to be Gaussian) by the relation: $S_\lambda = 2[2\ \ln(2)]^{0.5}\sigma_\lambda = 2.35\sigma_\lambda$. Moreover, S_λ is related to the base of the predicted triangular distribution $\Delta\lambda$ by the relation: $\sigma_\lambda = 2[\ln(2)/\pi]^{0.5}\Delta\lambda = 0.94\Delta\lambda$ obtained by equating the areas of these two peaked functions. Figs. 6c and 6d show representative runs above and below the Bragg cutoff for Bi. Runs with different neutron beam collimations: one with six neutron guides in (0.275° beam divergence) and one with no neutron guide in (0.093° beam divergence) showed that beam divergence has a negligible effect on the observed width.

The result of our fits to the data is:

$$\lambda_0[\text{Å}] = 0.18 + (2.610 \times 10^4 + 3.86 \times 10^3\nu)/\omega[\text{rpm}]$$

which represents the "calibration curve". Compared to the predicted relationship:

$$\lambda_0[\text{Å}] = (3.138 \times 10^4 + 3.74 \times 10^3\nu)/\omega[\text{rpm}],$$

the experimentally determined results show a 17% discrepancy.

8. Conclusions

Three multidisk selectors have been purchased from Transelektro, Hungary [8] for use on SANS instruments at the NIST-CNRF. After technical modifications (redesign of the bearing configuration, and replacement of the dc motors and their driving electronics) these selectors have been operating reliably. Tests on the first two selectors, performed earlier, gave wavelength calibration curves that agreed with prediction (based on design parameters) to within 6%, but the results for the third selector differ by 17%. This fact is not yet understood. A number of factors may be the cause of this discrepancy: a slight tilt of the rotor (by about 1.5°) with respect to the outside housing (which is used to align the selector parallel to the neutron beam), inaccuracy of the rotation speed, inaccuracy of the helix pitch angle, of the window openings, of the absorbing regions, etc. The second possibility has been excluded by checking the speed with a tachometer, while the other possibilities will be investigated in the future.

After extensive testing of the multidisk selectors, it is concluded that they perform adequately within the range of wavelength and wavelength spreads required for our application (SANS) after the technical modifications mentioned earlier and after careful wavelength calibrations. Moreover, our preliminary modeling and subsequent experimental tests have shown that these selectors can function in the "reverse" mode.

Schemes of distributing the disks along the neutron path (other than the Rosta design) can be envisaged. Schemes based on more than one transmitting/absorbing channel are more efficient in the sense that they give lower coverage (than the present design where on the average 5.5 absorbing layers are stacked in the path of wrong wavelength neutrons).

Another method based on acceptance diagrams (commonly used to determine the transmission of neutron guides) has also been pursued [10] in order to model multidisk selectors as a series of absorbing masks and transmitting windows. This method has many advantages over the ray tracing method used here.

Acknowledgements

Many discussions with Dr. J.R.D. Copley as well as his efforts in helping us think through some of the issues discussed in this paper are duly acknowledged. Mr. M. Dalle's (CEN-Saclay, France) coaching during the bearing modifications to our selectors was vital to our technical staff. Drs. C.J. Glinka and J. Barker's help during the wavelength calibrations, Dr. D.F.R. Mildner's help in improving the manuscript and Dr. M.J. Rowe's guidance in this project are greatly appreciated. A few discussions with Dr. L. Rosta were also helpful.

References

[1] J.G. Dash and H.S. Sommers Jr., Rev. Sci. Instr. 24 (1953) 91.

[2] R.D. Lowde, J. Nucl. Energy A11 (1960) 69.

[3] C.D. Clark, E.W. Mitchell, D.W. Palmer and I.H. Wilson, J. Sci. Instr. 43 (1966) 1.

[4] L. Rosta, G.Y. Zsigmond, B. Farago, F. Mezei, K. Ban and J. Perendi, KFKI Report 79/E (1987), Central Research of Physics, Hungarian Academy of Sciences, Budapest.

[5] L. Rosta, Physica B156/157 (1989) 615.

[6] L. Rosta, KFKI Report 29/E (1988). Central Research of Physics, Hungarian Academy of Sciences, Budapest.

[7] R. Papoular, These de Doctorat d'Etat, Universite de paris VI, (1991).

[8] Certain equipment and instruments or materials are identified in this paper in order to specify the experimental conditions adequately. Such identification does not imply recommendation by the National Institute of Standards and Technology nor does it imply that the materials are necessarily the best available for the purpose.

[9] L. Rosta, private communication.

[10] J.R.D. Copley, private communication, 1991.